scientific reports



OPEN

Protective effect of compound K against podocyte injury in chronic kidney disease by maintaining mitochondrial homeostasis

Fugang Huang^{1,5}, Shuo Huang^{2,5}, Ke Sun³, Yanhao Chen¹, Guanqun Xie², Jie Bao² & Yongsheng Fan^{4 \boxtimes}

Chronic kidney disease (CKD) stands as a formidable global health challenge, often advancing to endstage renal disease (ESRD) with devastating morbidity and mortality. At the central of this progression lies podocyte injury, a critical determinant of glomerular dysfunction. Compound K (CK), a bioactive metabolite derived from ginsenoside, has emerged as a compelling candidate for nephroprotective therapy. Here, we unveil the profound therapeutic potential of CK in a folic acid (FA)-induced CKD mouse model, demonstrating its ability to restore renal function and mitigate podocyte injury. CK exerted its nephroprotective effects by reinforcing inter-podocyte junctions, suppressing aberrant podocyte motility, and preventing podocyte detachment and apoptosis, thereby safeguarding the glomerular filtration barrier. Mechanistically, we identified mitochondrial dysregulation as a key driver of excessive oxidative stress, which is commonly associated with podocyte damage. CK remarkably restored mitochondrial homeostasis by attenuating pathological mitochondrial fission and enhancing mitophagy, thereby rebalancing the delicate mitochondrial network. Intriguingly, CK may disrupt the formation of the Drp1-Bax dimer, a crucial mediator of mitochondrial apoptosis, further averting podocyte loss. Collectively, our findings highlight CK as a potent nephroprotective agent, offering a novel therapeutic avenue for CKD management and redefining possibilities in the battle against progressive renal disease.

Keywords Chronic kidney disease, Compound K, Podocyte Injury, Apoptosis, Mitochondrial homeostasis

Chronic kidney disease (CKD) is a progressive disorder marked by sustained renal structural and functional impairments. It often culminates in end-stage renal disease and contributes to significant morbidity and mortality¹. A growing body of evidence underscores the role of acute kidney injury (AKI) as a pivotal precursor to CKD, shifting the perception of AKI from a reversible insult to a significant risk factor for chronic renal pathology². The transition from AKI to CKD involves complex maladaptive repair mechanisms, including persistent inflammation, fibrotic remodeling, and ongoing cellular injury, which, if unresolved, drive the progression towards irreversible kidney damage³. This AKI-to-CKD continuum highlights a critical therapeutic window wherein early intervention could potentially mitigate the long-term sequelae of AKI^{4,5}.

Despite advancements in nephrology, therapeutic options for CKD remain limited, making the exploration of novel interventions imperative. CK, a bioactive metabolite derived from the enzymatic transformation of ginsenosides by gut microbiota, has garnered significant attention due to its superior bioavailability and pharmacokinetics compared to its parent compounds⁶. CK possesses potent anti-inflammatory, antioxidant, and immunomodulatory properties, which are instrumental in counteracting the pathological processes underlying kidney injury. In preclinical models of kidney disease, CK has shown remarkable efficacy in reducing proteinuria and ameliorating histopathological damage, particularly in conditions such as diabetic nephropathy (DN) and IgA nephropathy (IgAN)^{7,8}. Moreover, CK has demonstrated substantial antifibrotic effects in CKD models by

¹The First School of Clinical Medicine, Zhejiang Chinese Medical University, Hangzhou, People's Republic of China. ²School of Basic Medical Sciences, Zhejiang Chinese Medical University, Hangzhou, People's Republic of China. ³The Third School of Clinical Medicine, Zhejiang Chinese Medical University, Hangzhou, People's Republic of China. ⁴The Second Affiliated Hospital of Zhejiang Chinese Medical University, Hangzhou, People's Republic of China. ⁵Fugang Huang and Shuo Huang have contributed equally to this work and share first authorship. [™]email: fysszjtcm@163.com

modulating key molecular pathways implicated in renal fibrosis. Specifically, CK attenuates the nuclear factor kappa-B (NF- κ B) and signal transducer and activator of transcription 3 (STAT3) signaling cascades, which are involved in the activation of the NLR family pyrin domain-containing protein 3 (NLRP3) inflammasome, thereby suppressing inflammation. Concurrently, CK inhibits the transforming growth factor- β (TGF- β)/mothers against decapentaplegic homolog (Smad) axis, a central pathway in the fibrogenic process, thus decelerating the progression of renal fibrosis. While CK's renoprotective effects have been well-documented, particularly in chronic stages of kidney disease, the intricate mechanisms through which CK exerts its influence during the critical AKI-to-CKD transition remain largely unexplored.

Podocytes, highly specialized epithelial cells, are a critical component of the glomerular filtration barrier (GFB). Their dysfunction or loss is a major driver of proteinuria and glomerulosclerosis, conditions that significantly contribute to the progression of renal diseases¹⁰. Importantly, podocyte injury is often one of the earliest manifestations of CKD, marking the beginning of an accelerated decline in renal function, a key hallmark of CKD development¹¹.

Under normal physiological conditions, podocytes play a crucial role in maintaining the integrity of renal filtration through their foot processes (FPs), which adhere to the glomerular basement membrane (GBM). These FPs form complex interdigitating structures that create the slit diaphragm (SD), a selective filtration barrier essential for maintaining proper kidney function¹². The functionality of podocytes, therefore, is highly dependent on the maintenance of their structural integrity¹³. However, podocytes are particularly sensitive to various stressors and are prone to damage^{14,15}. During CKD progression, factors such as glomerular hypertension and hyperfiltration exert tremendous mechanical and biochemical stress on podocytes, leading to FP effacement and collapse of the SD. These structural disruptions precipitate podocyte detachment, which triggers a cascade of failures in the filtration mechanism. This not only results in the leakage of essential macromolecules like albumin but also accelerates the overall progression of CKD^{11,16}.

Apoptosis, a key mechanism of programmed cell death in podocytes, often occurs following detachment^{17,18}. In CKD, podocytes are exposed to various stimuli, including oxidative stress¹⁹, endoplasmic reticulum stress²⁰, inflammatory responses²¹, angiotensin II²², and elevated homocysteine levels²³, with excessive oxidative stress being the most prevalent factor. Mitochondrial homeostasis imbalance is a critical driver of oxidative stress overload in podocytes, initiating a cascade of deleterious changes. Damaged mitochondria exhibit disruptions such as electron transport chain (ETC) complex dysfunction^{24,25}, cristae structural remodeling²⁶, reduced mitochondrial biogenesis²⁷, and metabolic reprogramming²⁸. Among these, reactive oxygen species (ROS) leakage—a byproduct of ETC activity—plays a dominant role in exacerbating oxidative stress.

Mitochondrial dynamics and mitophagy are pivotal processes in maintaining mitochondrial homeostasis, to safeguard podocyte function²⁹. However, disruptions in mitochondrial dynamics are closely linked to stress-induced mitochondrial damage^{29,30}. In CKD-related conditions such as DN and membranous nephropathy (MN), excessive mitochondrial fission and fragmentation have been consistently observed, correlating strongly with severe podocyte injury^{14,31,32}. Dynamin-related protein 1 (Drp1), a central regulator of mitochondrial fission, is recruited to the outer mitochondrial membrane (OMM) by factors like Fission 1 (Fis1) to mediate mitochondrial segmentation^{29,30}. Aberrant Drp1 activation amplifies mitochondrial fragmentation, exacerbating podocyte dysfunction. Notably, inhibition of Drp1 activity has been shown to mitigate mitochondrial damage and alleviate podocyte injury^{22,33,34}. Furthermore, Drp1 interacts with the pro-apoptotic protein Bcl-2-associated X protein (Bax) to form pores on the OMM, facilitating cytochrome c (cytc) release and activating the cysteine-aspartic acid protease 3 (caspase-3) apoptotic cascade³⁵.

Mitophagy, a specialized form of autophagy targeting damaged mitochondria, is critical for maintaining mitochondrial homeostasis and preventing cellular damage³⁶. In the context of CKD, especially during podocyte injury, decreased levels of mitophagy have been observed, coinciding with disruptions in mitochondrial dynamics and an increased cellular stress response^{37–39}. The interplay between mitophagy and mitochondrial dynamics is essential for regulating apoptosis, underscoring the importance of mitophagy in preserving mitochondrial integrity and cellular viability^{40–44}.

Building on this understanding, the present study aims to evaluate the nephroprotective potential of CK in a FA-induced CKD model and investigate whether CK alleviates GFB dysfunction by mitigating podocyte injury. Beyond its protective effects, we explore the potential mechanisms, hypothesizing that CK may modulate excessive oxidative stress—a central contributor to podocyte damage—arising from mitochondrial homeostasis disruption. Specifically, we focus on two pivotal aspects of mitochondrial regulation, mitochondrial dynamics and mitophagy, to uncover the mechanisms underlying CK's renoprotective effects and provide novel insights into its therapeutic potential for combating CKD progression.

Results

CK ameliorated renal injury in FA-induced mice

This study employed a well-established CKD model, induced by folic acid (FA), to evaluate the therapeutic potential of CK ($20-O-\beta-D$ -glucopyranosyl-20(S)-protopanaxadiol, depicted in Fig. 1a) in mitigating renal injury ^{45,46}. As previously reported, days 7 and 14 post-FA administration best capture the pathological hallmarks of AKI and CKD⁴⁷. Therefore, CK was administered orally at specific doses for 7 and 14 consecutive days, as outlined in Fig. 1b.

At both assessment points, the FA-induced model group exhibited significantly elevated proteinuria, serum creatinine (SCr), and blood urea nitrogen (BUN) levels compared to the control group, indicating progressive renal deterioration (Fig. 1c-d). Notably, these renal biomarkers showed marked improvement following CK treatment. A parallel trend was observed in the reduction of pro-inflammatory cytokine levels in the serum, as illustrated in Fig. 1e. Histopathological analysis revealed profound renal structural damage in the model group at both time intervals, including glomerular disarray, mesangial cell hyperplasia, crescent formation, and

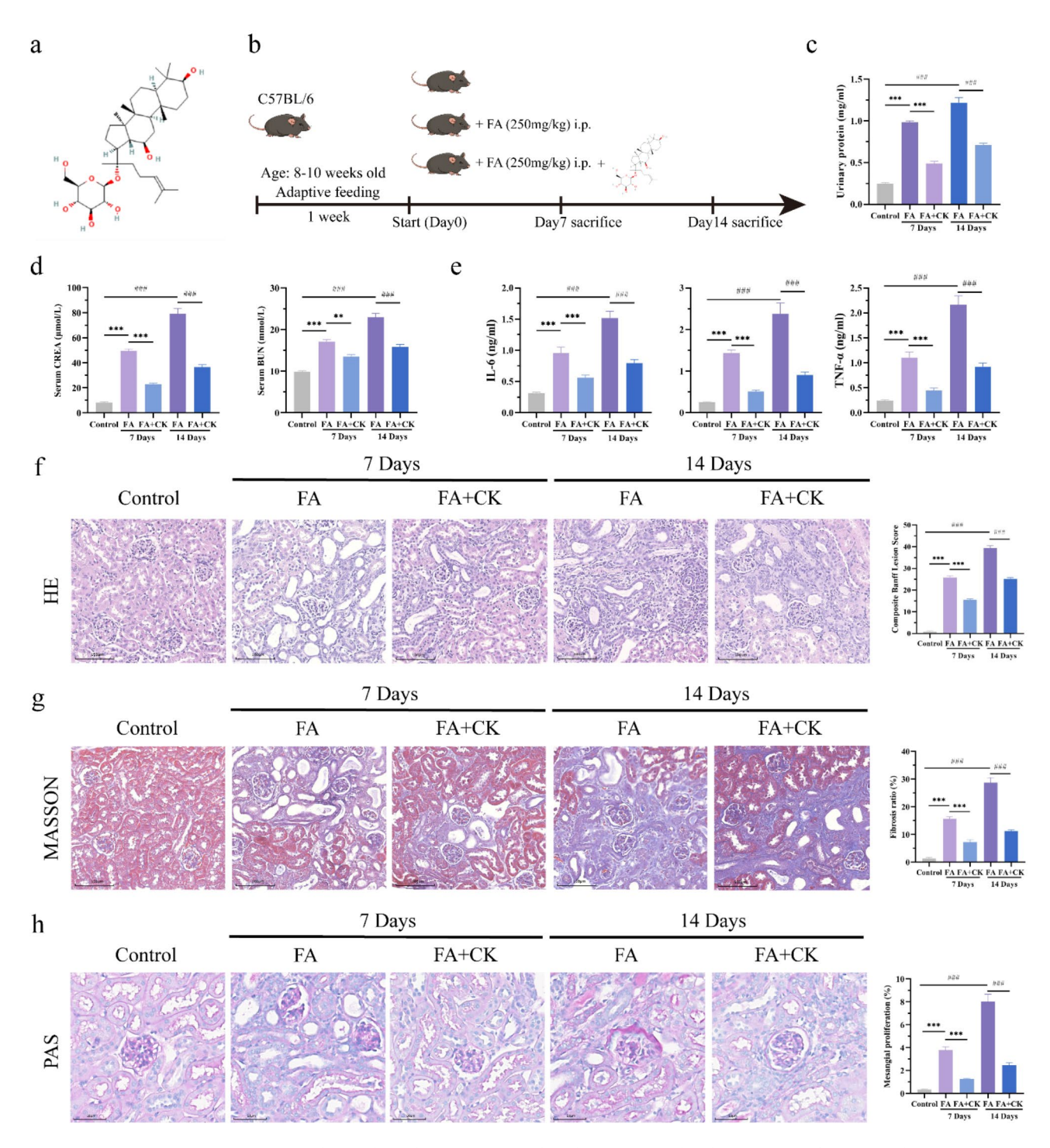


Fig. 1. CK ameliorated renal injury in FA-induced mice. (a) Molecular structure of CK. (b) Schematic representation of the experimental design for animal studies. (c-d) Levels of proteinuria, SCr, and BUN in the different groups. (e) Concentrations of circulating inflammatory factors, including IL-6, IL-1β, and TNF-α. (f-h) Representative images of kidney sections stained with H&E, Masson's trichrome, and PAS to assess renal histopathology (scale bars: 100 μm for H&E and Masson's trichrome, 50 μm for PAS), with corresponding quantitative analysis. Data are expressed as mean ± SD. Statistical significance is indicated as $^*P < 0.05$, $^*P < 0.01$ versus 7-day FA group; $^*P < 0.05$, $^*P < 0.01$ versus 14-day FA group. Abbreviation: IL-6, interleukin-6; IL-1β, interleukin-1 beta; TNF-α, tumor necrosis factor-alpha.

extensive inflammatory cell infiltration. Furthermore, the model group demonstrated a pronounced increase in renal fibrosis, characterized by excessive collagen deposition and marked thickening of the basement membrane (Fig. 1f-h). Although the severity of pathological alterations intensified over time, CK treatment significantly ameliorated these effects, underscoring its protective potential in the FA-induced CKD model.

CK restored podocyte injury

Given the severe kidney damage observed at day 14 and CK's notable nephroprotective effects, we conducted a transcriptome analysis of kidney tissues to explore the underlying genetic changes. CK treatment significantly downregulated genes related to lamellipodium formation, cell motility, and actin cytoskeleton organization compared to the model group (Fig. 2a,b). Podocytes, which play a critical role in renal filtration, rely on the integrity of their FPs and stable actin cytoskeleton. These findings prompted further investigation into whether podocyte alterations contributed to the observed renal injury.

Electron microscopy revealed marked deformation, retraction, and fusion of FPs in the model group at both time points. Additionally, basement membrane thickening indicated a breakdown of the filtration barrier. CK administration successfully reversed these morphological changes (Fig. 2c). We then examined the expression of Synaptopodin, an actin-binding protein essential for maintaining FP structure and protecting podocytes under stress⁴⁸, and Nephrin, a SD protein that links FPs and regulates intracellular signaling⁴⁹. Both proteins are critical for podocyte differentiation and stability. Western blot analysis showed significant reductions in these proteins in the model group, particularly on day 14. CK treatment countered this decline (Fig. 2d–f), a result further confirmed by immunofluorescence (Fig. 2g).

To validate CK's protective effects on podocytes, in vitro studies using lipopolysaccharide (LPS)-induced MPC-5 cells—a model for injured podocytes—were conducted. CK treatment showed no cytotoxicity and improved cell viability at concentrations of 1μM and 2μM after LPS exposure, demonstrating its therapeutic potential (Fig. 2h). LPS stimulation triggered a significant increase in the transcription of pro-inflammatory markers IL-6, IL-1β, and TNF-α. CK treatment attenuated these inflammatory responses (Fig. 2i). Additionally, CK reversed the LPS-induced downregulation of Synaptopodin (SYNPO), Nephrin 1 (Npsh1), and Nephrin 2 (Npsh2), which encode podocyte-specific proteins Synaptopodin, Nephrin, and Podocin, respectively (Fig. 2j).

CK suppressed reprogrammed actin cytoskeleton mediated podocyte motility

Excessive podocyte motility following FP effacement is another key aspect of podocyte injury, contributing to detachment⁵⁰. Transcriptome analysis revealed significant changes in the expression of cell motility-related genes following CK treatment. To further explore this, a scratch assay was performed to assess podocyte migration. Under LPS stimulation, podocytes covered nearly 70% of the scratch area, a significant increase compared to the control group. CK treatment reduced podocyte movement, stabilizing their dynamics (Fig. 2k). Podocyte motility is tightly regulated by actin cytoskeleton dynamics^{8,51}. Ras homolog family member A (RhoA), a key regulator of actin cytoskeletal dynamics⁵², influences podocyte morphology^{53,54}. LPS exposure increased RhoA activity, contributing to unfavorable changes in podocyte structure. CK treatment reduced RhoA transcription and increased the expression of Myosin IXA (Myo9A), a Rho-GAP protein that inhibits RhoA activity⁵⁵ (Fig. 2l). Furthermore, we investigated Nephrin's role in regulating the actin cytoskeleton through cofilin 1 (Cfl1), a protein involved in actin disassembly and reorganization. Although Cfl1 transcription levels remained unchanged across groups, CK preserved actin filament stability by modulating Cfl1-related regulators, slingshot homolog 1 (Ssh1) and LIM domain kinase 1 (Limk1). This stabilization of the cytoskeleton reduced LPS-induced podocyte motility (Fig. 2m).

CK reversed increased apoptosis and oxidative stress in podocytes

Apoptosis is a common destination when podocytes are injured and detach from the GBM. Transcriptome analysis revealed a significant downregulation of apoptosis-related genes following CK treatment (Fig. 3a,b). In the glomeruli of the model group, apoptosis levels were markedly elevated compared to the control group, particularly by day 14 (Fig. 3c). Additionally, the pro-apoptotic protein Bax and its downstream effector, cleaved caspase-3—an active form of caspase-3—were significantly upregulated in the model group at both examined time points. These observations indicate an increase in apoptotic activity, which was effectively mitigated by CK treatment (Fig. 3d-f).

Podocyte apoptosis often occurs in conjunction with disruptions in redox homeostasis, primarily driven by elevated oxidative stress. CK-treated kidneys exhibited significant enrichment in antioxidant-related gene expression (Fig. 3g,h). In vitro, LPS stimulation resulted in elevated malondialdehyde (MDA) levels and diminished superoxide dismutase (SOD) activity compared to controls. Notably, CK treatment successfully restored these parameters to near-normal levels (Fig. 3i). Excessive accumulation of intracellular ROS is a major contributor to heightened oxidative stress. In the model group, ROS-responsive genes were significantly downregulated (Fig. 3j,k). Moreover, LPS-treated podocytes exhibited a pronounced increase in ROS levels, which was markedly alleviated by CK administration (Fig. 3l,m). ROS is commonly generated from mitochondrial dysfunction triggered by the disruption of mitochondrial homeostasis. As byproducts of energy production, ROS are released into the cytoplasm following mitochondrial fragmentation, leading to oxidative stress and cellular damage. Further investigation of mitochondrial membrane potential (ΔΨm) revealed that LPS-treated cells displayed significantly enhanced green fluorescence, accompanied by a marked reduction in the red/green fluorescence ratio, indicating mitochondrial depolarization and membrane potential damage. Following CK treatment, green fluorescence was markedly reduced, red fluorescence was restored, and the red/green fluorescence ratio approached that of the control group, demonstrating that CK effectively restored mitochondrial membrane potential and mitigated mitochondrial damage (Fig. 3n,o). Together, these findings highlight the therapeutic potential of CK in protecting podocytes from apoptosis and preserving mitochondrial integrity under oxidative stress conditions.

CK maintained mitochondrial dynamics during podocyte injury

Recognizing the pivotal role of mitochondrial homeostasis in alleviating podocyte injury, we delved deeper into mitochondrial-related gene expression profiles. Although GSEA plots for mitochondrial dynamics—essential

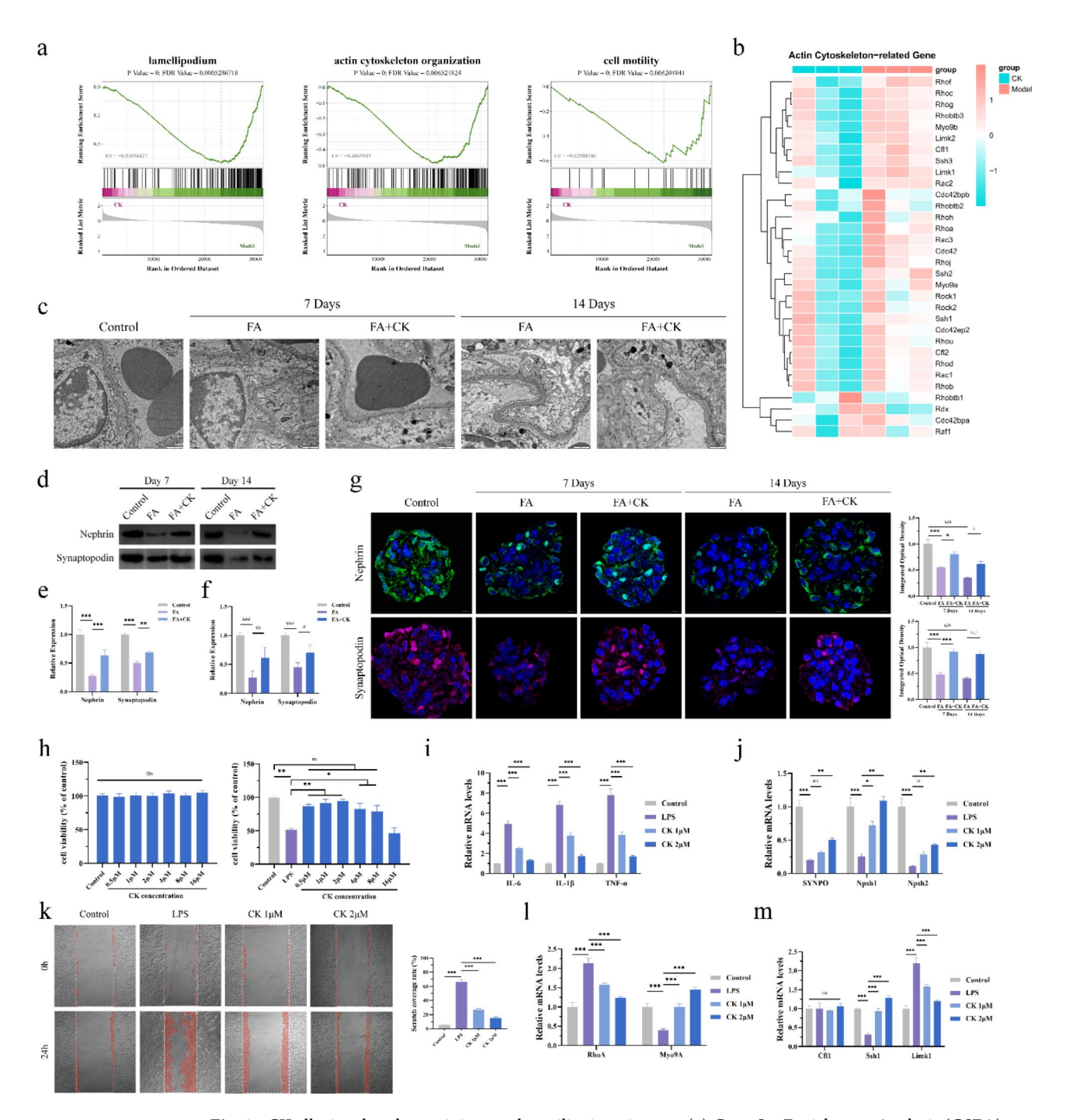


Fig. 2. CK alleviated podocyte injury and motility impairment. (a) Gene Set Enrichment Analysis (GSEA) plots: Left panel represents lamellipodium-related pathways, middle panel shows actin cytoskeleton organization, and right panel depicts cell motility. (b) Heatmap of actin cytoskeleton-related genes across experimental groups. (c) Microstructure of FPs visualized by transmission electron microscopy (TEM) (scale bars: 1 μm). (**d**–**f**) Western blot analysis with corresponding quantifications showing Nephrin and Synaptopodin expression in renal cortical samples; (e) depicts results at 7 days and (**f**) at 14 days. (**g**) Immunofluorescence staining of Nephrin and Synaptopodin in glomeruli, demonstrating protein localization and distribution (scale bars: 5 μm), with corresponding quantitative analysis. (**h**) Cell viability of podocytes treated with CK, with or without LPS stimulation, assessed quantitatively. (**i**) Transcription levels of proinflammatory cytokines IL-6, IL-1β, and TNF-α. (**j**) Transcription levels of SYNPO, Npsh1, and Npsh2. (**k**) Cell migration visualized by scratch assay, with quantification of wound area coverage after injury. (**l**–**m**) Transcription levels of RhoA, Myo9A, Cfl1, Ssh1, and Limk1 in MPC-5 cells stimulated by LPS. Data are presented as mean ± SD. Statistical significance is indicated as *P<0.05, *P<0.01 versus the 7-day FA group; *P<0.05, *P<0.01 versus the 14-day FA group. For in vitro experiments, *P<0.05, *P<0.01 versus the LPS-treated group.

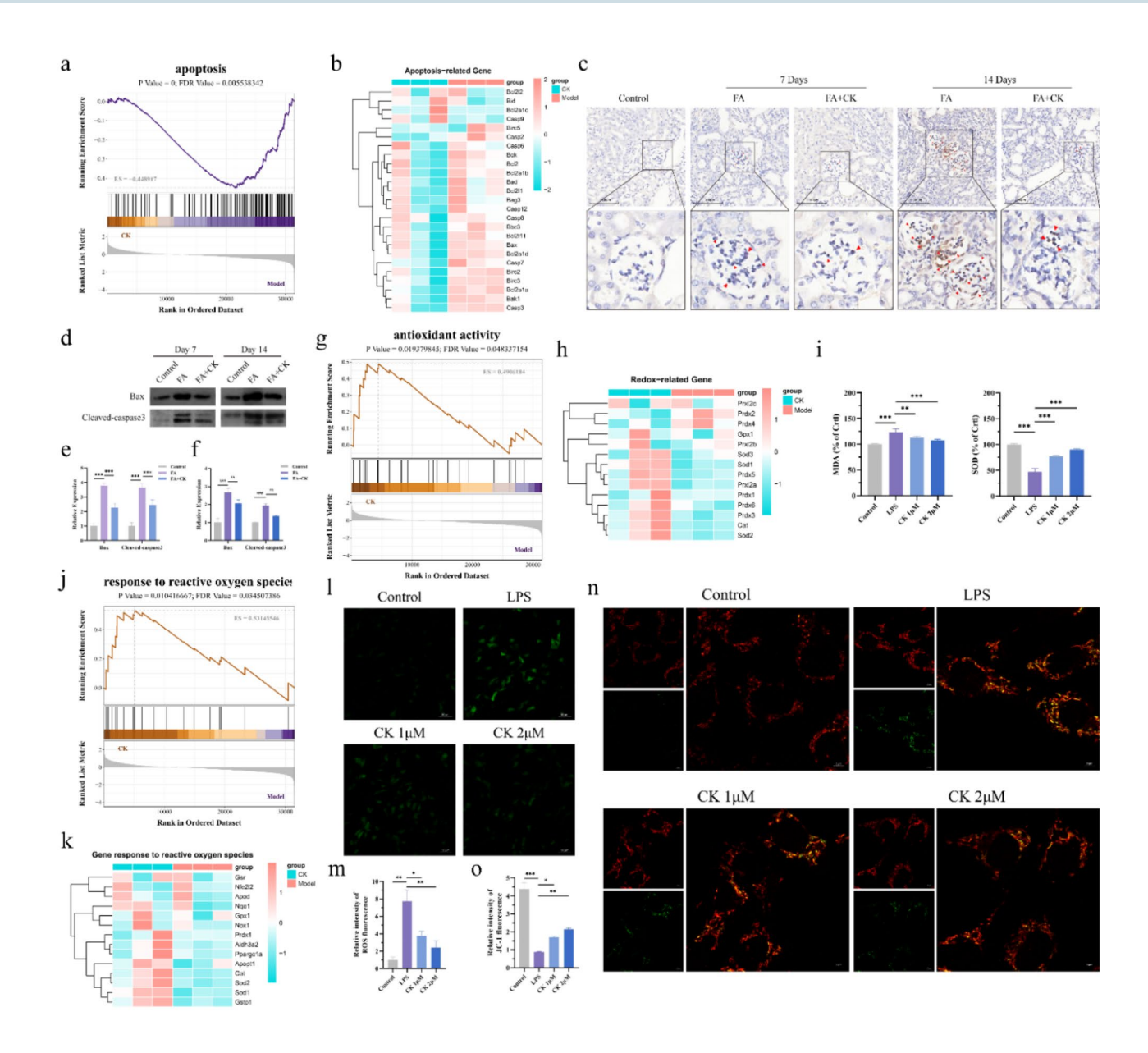


Fig. 3. CK protects against podocyte apoptosis and preserves mitochondrial integrity compromised by oxidative stress. (a) GSEA plots depicting pathways related to apoptosis. (b) Heatmap illustrating the expression of apoptosis-related genes. (c) TUNEL assay images demonstrating apoptotic cells across different groups (scale bars: $100 \, \mu m$). (d) Western blot analysis with corresponding quantification showing Bax and cleaved caspase-3 expression levels in renal cortical samples; (e) depicts results at day 7, and (f) at day 14. (g) GSEA plots illustrating pathways associated with antioxidant activity. (h) Heatmap of redox-related gene expression across groups. (i) Intracellular levels of MDA and SOD activity. (j) GSEA plots for genes involved in the response to ROS. (k) Heatmap showing the expression of ROS-responsive genes. (l,m) Representative images of ROS staining, with green fluorescence indicating the presence and distribution of ROS (scale bars: $50 \, \mu m$). (n,o) JC-1 staining images depicting alterations in $\Delta \Psi m$ (scale bars: $5 \, \mu m$). Green fluorescence represents JC-1 aggregates, indicative of high membrane potential. Quantification was performed based on the ratio of red to green fluorescence. Data are presented as mean ± SD. Statistical significance is indicated as *P < 0.05, **P < 0.01 versus the 7-day FA group; *P < 0.05, **P < 0.01 versus the LPS-treated group.

regulators of mitochondrial function—did not exhibit overt differences, heatmap analysis unveiled a striking dichotomy: the model group displayed a significant upregulation of fission-associated genes alongside a marked downregulation of fusion-related genes (Fig. 4a,b).

To further unravel the mitochondrial alterations, we investigated morphological changes specifically in LPS-stimulated podocytes. Damaged podocytes in the model group predominantly exhibited elongated, spindle-shaped mitochondria, in stark contrast to the compact, oval-shaped mitochondria characteristic of control cells. This pronounced increase in mitochondrial aspect ratio reflected a profound imbalance in mitochondrial dynamics, driven by excessive fission and impaired fusion. Remarkably, CK treatment induced a dose-dependent restoration of mitochondrial homeostasis, normalizing mitochondrial morphology, reducing the aspect ratio, and re-establishing mitochondrial network balance (Fig. 4c). Next, we evaluated the molecular mechanisms underpinning CK's effects, focusing on its interaction with Drp1, a master regulator of mitochondrial fission. Molecular docking studies revealed a binding energy of -8.1 kcal/mol, indicating a strong and specific interaction between CK and Drp1, positioning Drp1 as a promising therapeutic target for CK (Fig. 4d). Building on this, we explored Drp1's activity at the molecular level. Phosphorylation of Drp1 at Ser616 (p-Drp1 Ser616), its active fission-inducing form⁵⁶, was significantly elevated in the renal cortex of the model group, underscoring hyperactivation of mitochondrial fission. Intriguingly, CK treatment effectively attenuated this pathological upregulation (Fig. 4e). Similarly, Fis1, another critical mediator of fission, exhibited elevated transcriptional

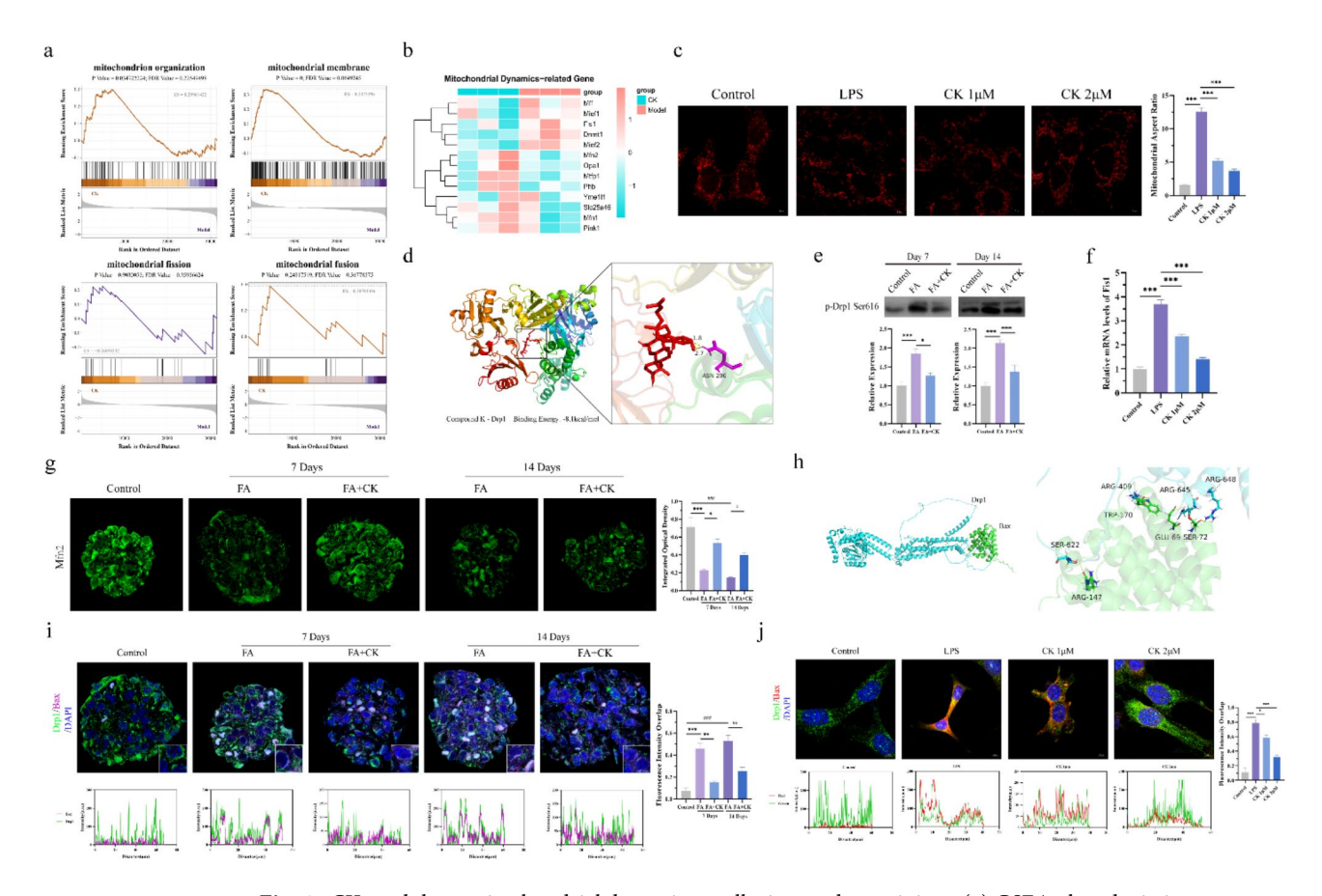


Fig. 4. CK modulates mitochondrial dynamics to alleviate podocyte injury. (a) GSEA plots depicting mitochondrial-related pathways, including mitochondrial organization, membrane integrity, fission, and fusion. (b) Heatmap illustrating the expression levels of genes associated with mitochondrial dynamics across experimental groups. (c) Representative images of mitochondrial morphology stained under different treatments (scale bar: 5 μm), with corresponding quantification of mitochondrial aspect ratio. (d) Molecular docking analysis of Drp1 and CK. (e) Western blot analysis of p-Drp1 Ser616, indicating mitochondrial fission activity, with quantification for both day 7 and day 14. (f) Relative mRNA levels of Fis1 in different groups. (g) Immunofluorescence staining of Mfn2 with corresponding quantification of expression levels (scale bar: 5 μm). (h) Structural interaction analysis of Drp1 and Bax, depicting key binding residues (e.g., Arg409, Arg645, Glu69, Ser72). (i) Immunofluorescence staining of Drp1 and Bax in glomeruli (scale bar: 5 µm), demonstrating their co-localization and relative expression, accompanied by line profile plots and quantification of colocalization. (j) Representative images of podocytes showing co-localization of Drp1 (green) and Bax (red) under different conditions (scale bar: 10 µm), with line profile plots and co-localization quantification. Data are expressed as mean \pm SD. Statistical significance is indicated as $^{*}P < 0.05$, $^{**}P < 0.01$ versus the 7-day FA group; $^{\#}P < 0.05, ^{\#}P < 0.01$ versus the 14-day FA group. For in vitro experiments, $^{*}P < 0.05, ^{**}P < 0.01$ versus the LPStreated group.

levels in injured podocytes, but CK administration suppressed this aberrant expression (Fig. 4f). In contrast, mitofusin 2 (Mfn2), a fusion-promoting protein severely downregulated in the model group, was restored to near-control levels upon CK treatment, highlighting CK's capacity to simultaneously enhance mitochondrial fusion dynamics (Fig. 4g).

Notably, under apoptotic conditions, Drp1 interacts with Bax, promoting Drp1 recruitment to mitochondria and thereby enhancing mitochondrial fission. This interaction leads to mitochondrial outer membrane permeabilization (MOMP), facilitating the release of apoptogenic factors and accelerating apoptosis. Through PISA (Protein Interfaces, Surfaces and Assemblies) analysis, we identified a potential interaction interface between Drp1 and Bax, characterized by a highly favorable free energy change ($\Delta G = -11.9 \, \text{kcal/mol}$), suggesting thermodynamic stability. The interface was fortified by a network of interactions, including eight hydrogen bonds (e.g., Glu69 with Arg645), four salt bridges (e.g., Glu69 with positively charged residues), and hydrophobic interactions involving key residues such as Trp170 (Fig. 4h). To validate the physiological relevance of this interaction, we conducted immunofluorescence co-localization experiments. The results revealed a pronounced increase in Drp1-Bax co-localization within the glomeruli of the model group, underscoring enhanced interaction under stress conditions. Strikingly, CK treatment contributed to reduce this co-localization, restoring the spatial segregation of these proteins (Fig. 4i). Further in vitro studies corroborated these findings, demonstrating that CK effectively disrupted the pathological association between Drp1 and Bax (Fig. 4j).

Collectively, these findings suggest that CK may play a multifaceted role in supporting mitochondrial dynamics. By potentially targeting Drp1 and modulating its interaction with Bax, CK appears to contribute to the maintenance of mitochondrial homeostasis, reducing excessive mitochondrial fragmentation and supporting cellular integrity. These results provide promising insights into the potential of CK as a therapeutic candidate for alleviating mitochondrial dysfunction and protecting against podocyte injury.

CK modulated autophagy/mitophagy

Mitophagy and mitochondrial dynamics are tightly interlinked processes, essential for maintaining mitochondrial quality control and cellular homeostasis. Although GSEA results did not reveal significant differences between the groups, expression levels of autophagy and mitophagy-related genes suggested increased autophagic and mitophagic activity in the model group (Fig. 5a,b). To further elucidate the status of autophagy, we assessed the expression of key autophagy biomarkers. Contrary to expectations, immunohistochemical analysis revealed elevated levels of p62 and reduced levels of Beclin-1 in the model group, changes that were effectively mitigated by CK treatment (Fig. 5c).

p62/SQSTM1, a cargo protein that forms complexes with classical autophagosome markers like microtubule-associated protein 1 light chain 3 (LC3), is involved in autophagosome-lysosome degradation. Notably, its accumulation in the cytoplasm is often indicative of impaired autophagic flux or inhibited autophagy^{57(p. 6)}. Beclin-1, a principal initiator of autophagy, facilitates the recruitment of autophagy-related proteins at pre-autophagosomal structures, serving as a critical factor in autophagy initiation⁵⁸. The observed alterations in p62 and Beclin-1 levels indicated a suppression of autophagy in the model group.

To gain deeper insights, we conducted immunofluorescence analysis, which demonstrated a reduced colocalization of LC3B, a key subtype of the LC3 protein family, with the lysosomal marker lysosome-associated membrane protein 1 (Lamp1), as well as diminished co-localization of Lamp1 with the mitochondrial marker translocase of the outer mitochondrial membrane 20 (TOM20) in the glomeruli of the model group. Additionally, the overall expression of LC3B within the model group's glomeruli showed a declining trend, further supporting the inhibition of autophagy and mitophagy in diseased glomeruli (Fig. 5d). These findings underscore a disruption in autophagic and mitophagic processes under pathological conditions, and highlight the potential of CK treatment to restore these essential cellular mechanisms.

Discussion

This study provides strong evidence for the renoprotective effects of CK, as it not only alleviated proteinuria but also significantly reduced SCr and BUN levels, improved renal histopathological damage, and delayed CKD progression in a FA-induced model. These findings are consistent with prior observations of CK efficacy in the unilateral ureteral obstruction (UUO) model⁴⁴. The FA model simulates the progression from AKI to CKD, where FA induced tubulointerstitial-glomerular feedback mechanism, leading to glomerular sclerosis that further damage the nephron, resulting in secondary progressive glomerulosclerosis⁴⁷. In this process, podocyte injury plays a key role in the progression of focal segmental glomerulosclerosis (FSGS). Podocytes, as epithelial cells of the glomerular capsule, undergo epithelial-to-mesenchymal transition (EMT), a fibrotic mechanism that leads to glomerulosclerosis and subsequent podocyte detachment. This leads to a state of glomerular hyperpressure, hyperperfusion, and hyperfiltration, where the mechanical and biological disturbances of the filtration membrane, along with hemodynamic changes, ultimately result in an imbalance of the glomerular filtration system. Notably, these changes trigger alterations in podocyte cytoskeleton dynamics, causing podocyte detachment and podocytopathy. Consistent with these findings, our model also showed that as AKI progressed to CKD, glomerular structural damage, mesangial proliferation, and renal fibrosis worsened, ultimately leading to the development of CKD. All of these pathological changes were ameliorated by CK treatment.

To further investigate the underlying mechanisms of CK's therapeutic effects in the CKD stage, we performed transcriptomic sequencing on kidneys harvested at day 14, corresponding to the CKD phase. The results indicated enrichment of pathways related to lamellipodium formation, cell motility, and actin cytoskeleton organization, all of which are characteristic of podocytes. Podocytes rely on their FPs to maintain the integrity of the GFB, and their function is highly dependent on the regulation of the actin cytoskeleton. Cytoskeletal reorganization, if dysregulated, can enhance podocyte motility, leading to detachment from the GBM and consequent reduction in GFR. Given the reported reciprocal relationship between tubular and glomerular damage in the FA model⁴⁷,

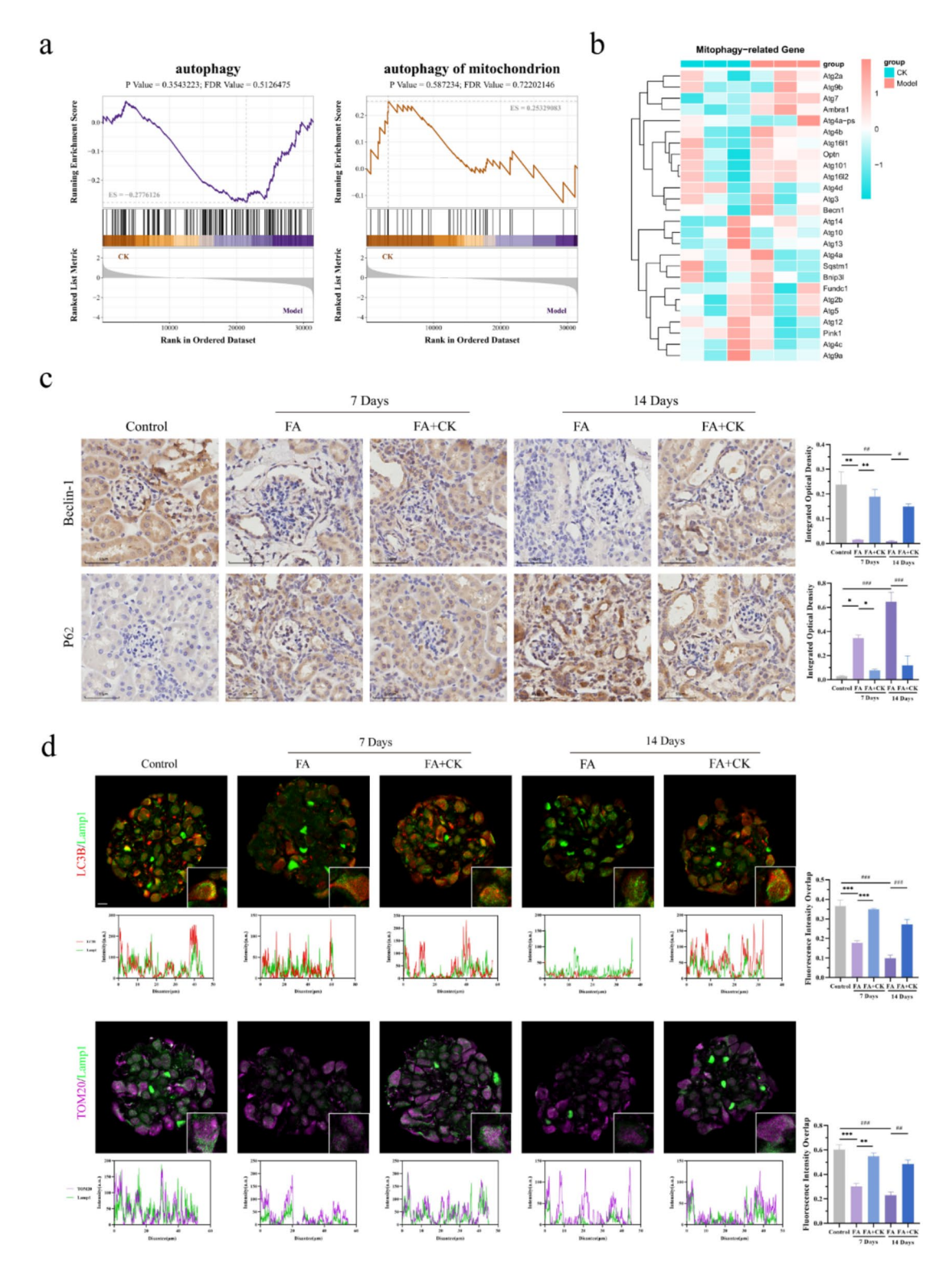


Fig. 5. CK modulated autophagy and mitophagy. (a) GSEA plots showing pathways related to autophagy and autophagy of mitochondria. (b) Heatmap depicting the expression profiles of mitophagy-related genes across experimental groups. (c) Immunohistochemical staining of Beclin-1 and p62, which are key autophagy markers (scale bar: 50 μ m), along with quantification of integrated optical density (IOD) to reflect changes in autophagic activity. (d) Immunofluorescence staining of LC3B and Lamp1 (top row), as well as TOM20 and Lamp1 (bottom row), in glomeruli at both 7-day and 14-day time points (scale bar: 5 μ m). Line profile plots represent the degree of co-localization, highlighting autophagosome formation (top) and mitophagy-related alterations (bottom). Corresponding quantitative analysis of fluorescence intensity overlap is shown on the right. Data are expressed as mean \pm SD. Statistical significance is indicated by *P<0.05, **P<0.01 versus the 7-day FA groups; *P<0.05, **P<0.01 versus the 14-day FA groups.

we explored CK's effects on podocyte function. Our findings confirmed that CK acts on damaged podocytes to preserve their phenotypic characteristics by maintaining the expression of podocyte-specific proteins such as Nephrin and Synaptopodin, thus preserving podocyte structural integrity. In vitro experiments further highlighted CK's ability to restrict podocyte motility. In examining key regulators of podocyte motility specifically cytoskeletal proteins—we measured the transcriptional levels of the cytoskeletal regulatory protein RhoA⁵⁹, its partner Myo9A, and the actin dynamics regulators Cfl1, Ssh1, and Limk1. The results demonstrated that CK corrected cytoskeletal dysregulation by inhibiting RhoA activity and upregulating Myo9A transcription. Cfl1, a critical regulator of podocyte actin dynamics, plays a key role in maintaining the normal architecture of actin filaments and FPs⁶⁰. Interestingly, while Cfl1 transcription remained stable, its functional activity depends on the dynamic interplay between its phosphorylated and non-phosphorylated forms. This regulation may not be reflected at the transcriptional level but is essential for podocyte function^{61,62}. Under normal physiological conditions, Cfl1 is activated through dephosphorylation mediated by its interaction with Nephrin, leading to reduced levels of phosphorylated Cfl1 (pCfl1)⁶³. However, during disease progression, such as in human glomerular diseases, elevated pCfl1 levels have been reported, likely due to the loss of Nephrin in damaged podocytes, resulting in reduced dephosphorylation of Cfl164. Although our study could not definitively determine the phosphorylation status of Cfl1, the transcriptional trends showing Ssh1 activation and Limk1 inhibition both of which regulate Cfl1 activity⁶⁵—suggest a potential shift towards increased phosphorylation in damaged podocytes. These findings underscore the need for further research to elucidate the specific phosphorylation/ dephosphorylation states of Cfl1 under CK treatment, providing deeper mechanistic insights into CK-mediated podocyte cytoskeletal reprogramming. In summary, CK helps remodel the podocyte cytoskeleton and fortifies its cell-cell and cell-matrix connections to restore SD integrity, counterbalancing the excessive shear and tensile stresses exerted on the glomerular vasculature by hyperfiltration. By fine-tuning podocyte actin dynamics, CK mitigates the mechanical stress-induced damage to the glomerular filtration barrier, offering a protective response to the destructive forces of glomerular hyperpressure and hyperfiltration.

Following the well-documented fate of podocyte detachment leading to cell death, we further investigated apoptosis within the transcriptomic data. Integrating our TUNEL assay and Western blot results, we confirmed that glomerular apoptosis was significantly suppressed after CK treatment. Oxidative stress is a well-known mediator of cell death, and in podocytes, increased oxidative levels can disrupt their cellular functions. Our enrichment analysis revealed that podocyte apoptosis was accompanied by increased oxidative stress, a finding that aligns with our direct measurements of oxidative stress in damaged podocytes. CK alleviated excessive oxidative stress, leading us to propose that CK may help promote podocyte survival and maintain normal function at least in part by modulating oxidative stress levels.

Excessive intracellular oxidative stress primarily arises from the overaccumulation of ROS, whose highly oxidative nature can inflict significant damage on podocytes⁶⁶. In our study, we observed a marked elevation in ROS levels within damaged podocytes, a phenomenon that was notably mitigated by CK treatment. While the increased ROS in the damaged state could stem from several molecular mechanisms, the most well-established pathway involves mitochondrial dysfunction. Here, ROS accumulate excessively as byproducts of the ETC when mitochondrial integrity is compromised. Additionally, ROS production may also be influenced by pathways such as endoplasmic reticulum (ER) stress, autophagic release, and the activation of NADPH oxidase (NOX)^{67,68}. Although these mechanisms may contribute to ROS generation, mitochondrial-derived ROS appear to be the primary driver of excessive oxidative stress. Therefore, our investigation seeks to elucidate the precise mechanisms by which CK alleviates oxidative stress, particularly focusing on its modulation of mitochondrial function.

Mitochondria are highly dynamic organelles, constantly undergoing renewal and remodeling, with the maintenance of mitochondrial homeostasis being essential for their proper function. Mitochondrial dynamics and mitophagy are two pivotal processes that govern this homeostasis. In our study, we identified a disruption in the delicate balance between mitochondrial fusion and fission, resulting in excessive mitochondrial fission. Specifically, when fusion is suppressed, fission is upregulated, leading to an over-fragmentation of mitochondria. This excessive fission can facilitate the release of ROS produced within the mitochondria into the cytosol, triggering oxidative stress, a key factor in podocyte injury. Interestingly, our results show that CK effectively mitigates this damage by inhibiting the expression of fission proteins and promoting the restoration of fusion proteins, thereby restoring the equilibrium of mitochondrial dynamics. Although previous research suggests that the regulation of mitochondrial fission proteins like Drp1 may be mediated through pathways such as SIRT1-PGC1α⁶⁹, it remains to be determined whether CK directly targets Drp1 or other specific proteins are involved. Nonetheless, our findings provide compelling evidence that CK has the potential to reverse mitochondrial dynamic imbalance, offering significant protection to podocyte function.

Of particular interest was our novel exploration of the complex formed between the fission protein Drp1 and Bax, as this complex has been reported to play a critical role in mitochondria-mediated apoptotic injury. Bax and Drp1 co-localize on mitochondria during apoptosis, orchestrating mitochondrial permeabilization and fragmentation. This process triggers the release of mitochondrial contents, such as ROS and cytc, into the cytosol, initiating a cascade of apoptotic signaling 35,70. The excessive production and release of ROS can destroy antioxidant defenses, enhance the pro-inflammatory potential of mitochondrial DNA⁷¹, or trigger the activation of inflammasomes, particularly the NLRP3 inflammasome, which may induce pyroptosis in podocytes^{72–74}. Cytc plays a crucial role in initiating the caspase-3 cascade, advancing the apoptotic process. Bax's ability to form membrane pores synergizes with the pro-apoptotic function of Drp1, which further amplifies Bax activity and its activation 35,75. Given the involvement of Drp1 in podocyte apoptosis, we sought to determine whether such interactions occur in our model. Our immunofluorescence co-localization analysis revealed a significant increase in the overlap of Bax and Drp1 in the model group, both in vitro and in vivo. Remarkably, CK treatment reduced this co-localization, with a pattern that mirrored the changes in apoptotic levels. These findings suggest

that the Drp1 and Bax may interact during podocyte damage to trigger apoptosis, and CK may influence this process, offering a protective effect that enhances podocyte function and safeguards glomerular filtration, ultimately serving as a powerful renal protective agent.

Mitophagy, a self-protective mechanism within cells, typically increases in response to cellular damage as a compensatory action, but this initial rise is usually followed by a reduction in activity over time⁴⁴. Although transcriptomic analysis indicated elevated autophagy levels in the renal tissues of the model groups, the diverging patterns observed through immunofluorescent co-localization of LC3B-Lamp1 and TOM20-Lamp1 within glomeruli suggest that these increases might reflect the activation of non-specific genes from multiple cell types. This accumulation likely extends beyond podocytes, possibly involving other renal cells such as tubular epithelial cells and macrophages, complicating the assessment of autophagy specifically in podocytes. Research by Hon-Kan Yi and colleagues has shown that renal tubular cells, due to their high energy demands for reabsorption, maintain a significantly larger mitochondrial reserve compared to other renal parenchymal cells, which influences overall autophagy assessments in diseased kidneys^{76,77}. Moreover, in renal injury scenarios marked by macrophage-dominant immune responses—including the infiltration of monocyte-derived macrophages and activation of tissue-resident macrophages—autophagy regulation is closely linked to the polarization and transformation of different macrophage phenotypes⁷⁸. The cumulative evidence strongly suggests that while general autophagy levels may appear increased, the specific autophagy/mitophagy activity in podocytes of FA-induced CKD mice is actually suppressed. However, administration of CK appears to enhance autophagy/ mitophagy, offering protective effects to podocytes. This differential response highlights the complexity of cellular interactions in the kidney and emphasizes the need for more targeted research to precisely understand the role of mitophagy in various cell types under pathological conditions. Nonetheless, our findings indicate that CK effectively restores the suppressed mitophagy in the glomeruli, a crucial mechanism that likely underpins its protective effects on renal function.

Conclusion

In conclusion, the evidence presented in this study demonstrates that CK significantly mitigates podocyte damage in the FA-induced CKD mouse model. CK achieves this by remodeling the actin cytoskeleton to reduce podocyte motility and stabilize its structural integrity, thereby improving glomerular filtration barrier function and delaying the progression of renal dysfunction and tissue pathological damage. Furthermore, CK effectively attenuates the excessive oxidative stress associated with podocyte injury and stabilizes the underlying factor contributing to this effect—disruption of mitochondrial homeostasis. Specifically, CK restores mitochondrial homeostasis by balancing mitochondrial dynamics, enhancing mitophagy, and potentially modulating the Drp1-Bax complex formation, which in turn reduces apoptosis. These findings elucidate the potential mechanisms by which CK exerts protective effects on podocyte function and contributes to the preservation of kidney health in CKD (Fig. 6).

Material and methods Animal experiments

Male C57BL/6 mice (aged 8–10 weeks, weighing 20–25 g) were obtained from Shanghai SLAC Laboratory Animal Co., Ltd. (Shanghai, China) and approved by the Institutional Animal Care and Use Committee (IACUC approval number: IACUC-20240429-16). All mice were housed under specific pathogen-free (SPF) conditions at 22±2 °C with 55±5% humidity and were provided unrestricted access to standard laboratory chow and tap water. A CKD model was induced in the model group via a single intraperitoneal injection of 250 mg/kg folic acid (FA, Sigma-Aldrich, St. Louis, MO, USA) dissolved in 0.2 mL sodium bicarbonate solution. The control group received an equivalent volume of sodium bicarbonate solution by intraperitoneal injection. Mice in the treatment group were orally gavaged with CK at a dose of 50 mg/kg, dissolved in 0.1 mL sterile PBS, starting on the day of model induction. All mice were sacrificed on days 7 and 14 by intraperitoneal injection of pentobarbital sodium (100 mg/kg), and tissue samples were collected for further analysis. All animal procedures were adhered to internationally accepted standards for animal research, following the 3Rs principle. The ARRIVE guidelines were employed for reporting experiments involving live animals, promoting ethical research practices. The use of laboratory animals has been approved by the Institutional Animal Care and Use Committee of Zhejiang Chinese Medical University.

Renal function evaluation

Renal function was evaluated by measuring proteinuria, BUN, and SCr levels. Urine specimens and serum samples were obtained. Following the manufacturer's instructions, proteinuria, BUN, and SCr levels were measured using commercially available kits (Nanjing Jiancheng Corp., China).

Enzyme-linked immunosorbent assay (ELISA)

Serum concentrations of IL-6, IL-1 β , and TNF- α were quantified using ELISA kits (Ruixinbio, Quanzhou, China).

Histopathological examination

Kidneys were excised, immediately fixed in a 4% paraformaldehyde buffered solution, and embedded in paraffin following a minimum of three days of fixation. Sections (4 µm thick) were subsequently stained with hematoxylin and eosin (H&E), Masson's trichrome, and periodic acid-Schiff (PAS). The H&E staining results were assessed using the Banff classification to evaluate kidney pathology. Quantitative analysis of the area stained by Masson's

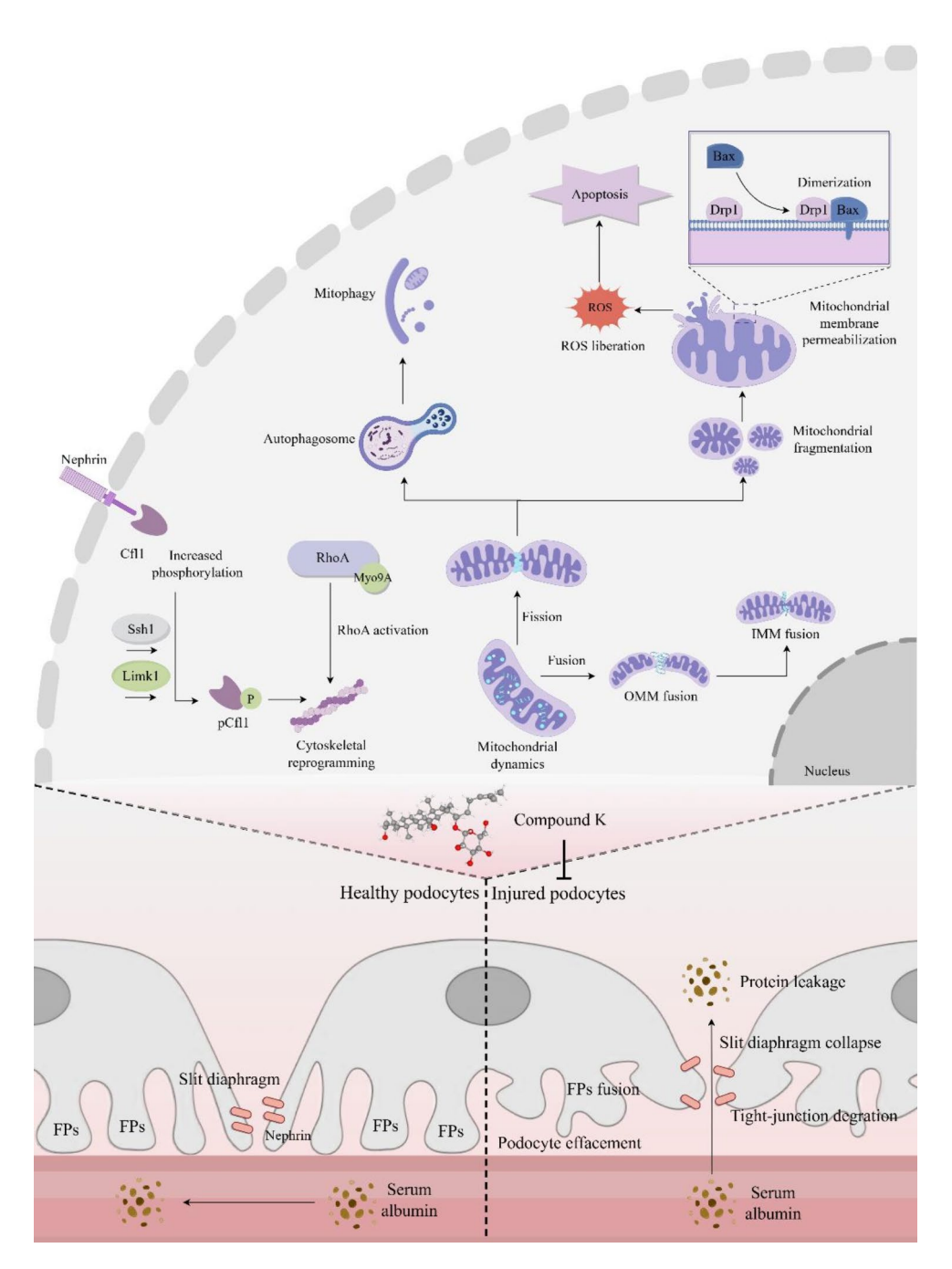


Fig. 6. Diagram illustrating an underlying mechanism of the potential therapeutic effect of CK against CKD.

trichrome and the proportion of PAS-positive basement membrane thickening was conducted using ImageJ software (Bethesda, MD, USA).

Transcriptome sequencing

Transcriptome sequencing was employed to analyze gene expression changes in kidney tissues from mice in the model group and those treated with CK. Total RNA was extracted from the tissues and its quality was evaluated. The RNA quality and purity were assessed using the Bioanalyzer 2100 and RNA 6000 Nano LabChip

Gene	Alias	Forward	Reverse
Interleukin-6	IL-6	TAGTCCTTCCTACCCCAATTTCC	TTGGTCCTTAGCCACTCCTTC
Interleukin-1β	IL-1β	GTACAAGGAGAACCAAGCAA	CCGTCTTTCATTACACAGGA
Tumor necrosis factor-α	TNF-α	CCCTCACACTCAGATCATCTTCT	GCTACGACGTGGGCTACAG
Nephrosis 1	Nphs1	ATGGGAGCTAAGGAAGCCACA	CCACACCACAGCTTAACTGTC
Nephrosis 2	Nphs2	GCATCAAGCCCTCTGGATTAG	AGACGGAGATCAACCTTGTGATA
Synaptopodin	Synpo	TCCTCACCTAATGCCACACTC	GCTGGAGGGTTTTGGTTGATA
Slingshot 1	Ssh1	CAGCGATGAAGAACGGAAATTG	GGTCGGTCCAGACACTCTCT
LIM-domain containing protein kinase 1	Limk1	ATGAGGTTGACGCTACTTTGTTG	CTACACTCGCAGCACCTGAA
Cofilin 1	Cfl1	ATGACATGAAGGTTCGCAAGT	GATAAAAGTGGTGTAGGGGTC
Ras homolog family member A	RhoA	AGCTTGTGGTAAGACATGCTTG	GTGTCCCATAAAGCCAACTCTAC
Myosin IXA	Myo9A	TCTGAGAAGTAGCAGGAATGC	AGCAACCACAGCTCTGAAA
Mitochondrial Fission 1 Protein	Fis1	TGTCCAAGAGCACGCAATTTG	CCTCGCACATACTTTAGAGCCTT
Glyceraldehyde-3-phosphate dehydrogenas	GAPDH	AATGGATTTGGACGCATTGGT	TTTGCACTGGTACGTGTTGAT

Table 1. Primers used for RT-PCR.

Kit (Agilent, CA, USA, 5067 – 1511). High-quality RNA samples, with RNA Integrity Number (RIN) values greater than 7.0, were selected for sequencing library construction. Sequencing was performed on the Illumina NovaSeq 6000 platform, generating 150 bp paired-end reads. The raw sequencing data were processed to remove low-quality reads and adapters, resulting in clean reads. These clean reads were aligned to the mouse reference genome using a suitable aligner, ensuring accurate mapping of the transcripts. Differential gene expression analysis was conducted using DESeq2, a robust statistical package designed for RNA-Seq data. Genes with a false discovery rate (FDR) of less than 0.05 were considered significantly differentially expressed. These genes were further analyzed to elucidate the molecular mechanisms underlying the effects of CK treatment, providing insights into potential therapeutic pathways.

Transmission electron microscopy (TEM)

Kidney cortex samples were dissected into 1 mm³ fragments and fixed in 2.5% glutaraldehyde in phosphate-buffered saline (PBS). Post-fixation, the samples were treated with 1% osmium tetroxide for 1 h, dehydrated in ethanol, and embedded in Spurr's epoxy resin. Ultrathin Sect. (70 nm) were prepared, stained with uranyl acetate and lead citrate, and examined with a JEOL JEM-2100 transmission electron microscope (Tokyo, Japan) to assess the ultrastructure of the FPs.

Western blot

Renal cortex were homogenized in RIPA buffer, which contained both protease and phosphatase inhibitors (Beyotime). Protein concentrations were determined using a BCA assay kit. Proteins were separated using SDS-PAGE (10%) and subsequently transferred to PVDF membranes. These membranes were blocked and then incubated with primary antibodies targeting Nephrin (Santa Cruz), Synaptopodin, Bax (both from Abcam), Cleaved-caspase3, and Phospho-Drp1 Ser616 (both from Cell Signaling Technology). Following the application of secondary antibodies (Cell Signaling Technology), protein bands were visualized using a Proteinsimple imager (CA, USA). Quantification was conducted using FluorChem FC3 software, with normalization of target proteins to GAPDH.

Cell culture and treatments

Immortalized mouse podocyte clone 5 (MPC-5) cells were sourced from Shanghai EK-Bioscience Biotechnology Co., Ltd. (Shanghai, China). Cells were cultured in high-glucose DMEM, supplemented with 10% fetal bovine serum (FBS) and antibiotics (100 μ g/mL streptomycin and 100 U/mL penicillin G) at 37 °C in a 5% CO2 atmosphere. Cells were fully differentiated before exposure to LPS (20 μ g/mL, Sigma-Aldrich) to induce stress conditions.

Cell viability assessment

Cell viability was assessed using the CCK-8 assay (Biosharp, Shanghai, China). Cells were seeded at a density of 5×10^3 per well in 96-well plates and allowed to adhere. Following adhesion, cells were treated with various concentrations of CK for 24 h. The CCK-8 solution (10 μ l) was added to each well and incubated for 1 h; absorbance at 450 nm was then measured to assess cell viability. This assay was also utilized to evaluate the effects of CK post-24-hour LPS induction.

RNA isolation and quantitative real-time PCR

Total mRNA was extracted from the stimulated cells utilizing RNAiso Plus (TaKaRa Biotechnology, Dalian, China). cDNA synthesis was conducted using the PrimeScript™ RT kit (TaKaRa). Target gene expression was quantified via quantitative real-time PCR employing SYBR Premix Ex Taq (TaKaRa), with GAPDH serving as the reference gene. The sequences of the primers used are detailed in Table 1.

Immunofluorescence staining.

Embedded renal cortex was sliced into $4\mu M$ sections for immunofluorescence staining. Following antigen retrieval and blocking, the sections were incubated overnight at 4 °C with primary antibodies against Nephrin (Santa Cruz), Synaptopodin (Abcam), Mfn2 (Cell Signaling Technology), Bax (HuaBio, China), phospho-Drp1 Ser616 (Cell Signaling Technology), LC3B (Cell Signaling Technology), Lamp1 (Cell Signaling Technology) and Tom20 (Cell Signaling Technology). Next, the sections were incubated with the corresponding secondary antibodies for 1 h at room temperature and sealed with a DAPI-contained mounting medium.

Cultured podocytes were seeded onto round coverslips in 12-well plates. The stimulated cells were fixed with 4% paraformaldehyde, permeabilized with 0.1% Triton X-100, and then blocked with 5% bovine serum albumin (BSA). Primary antibodies against Bax and phospho-Drp1 Ser616 were then added to detect their presence. After incubation with the corresponding secondary antibody for 1 h, the samples were mounted in a medium containing DAPI. Images were captured using an LSM700 Carl Zeiss confocal microscope (Jena, Germany) to further investigate the Drp1-Bax interaction.

TdT-mediated dUTP nick end labeling (TUNEL)

Paraffin-embedded sections were dewaxed, hydrated, and treated with proteinase K to permeabilize cells for the detection of apoptosis. Sections were then exposed to hydrogen peroxide to inhibit endogenous peroxidase activity, followed by TUNEL staining to label DNA 3'-OH ends. After a DAB chromogenic reaction and nuclear counterstaining, regions exhibiting positive TUNEL staining were analyzed using ImageJ software (Bethesda, MD, USA).

Scratch assay

Cells were seeded in 6-well plates and permitted to adhere. A scratch was created across the cell monolayer utilizing a 200 µl pipette tip. Following the removal of debris with a serum-free medium, cell migration into the scratch was documented at 0 and 24 h with a phase-contrast microscope (Olympus IX71, Japan).

Immunohistochemistry

Kidney sections underwent processing for immunohistochemistry, initially involving antigen retrieval and blocking. Sections were then incubated overnight at 4 °C with primary antibodies targeting P62 and Beclin-1. Following incubation with secondary antibodies and a DAB chromogen reaction for color development, sections were then counterstained for nuclei, dehydrated, and cover-slipped. Observations and image capture were conducted using a light microscope.

Membrane potential assays

Mitochondrial membrane potential, a crucial indicator of early apoptosis, was evaluated using JC-1, a sensitive fluorescent probe. Upon attaining confluence, podocytes were treated with a JC-1 staining solution. Following a 20-minute incubation at 37°C, the solution was aspirated, the wells were cleansed, and fresh culture medium was introduced. Subsequent fluorescence changes were monitored using an LSM700 Carl Zeiss confocal microscope (Jena, Germany).

Molecular docking

The chemical structure of Compound K was downloaded in SDF format (2D/3D structure) from the PubChem database (https://pubchem.ncbi.nlm.nih.gov) and converted to mol2 format using Open Babel GUI. The Drp1 protein structure was retrieved from the UniProt database (https://www.uniprot.org) as a PDB file and prepared in AutoDock Tools by removing water molecules, adding hydrogen atoms, and assigning Gasteiger charges. Molecular docking was performed using AutoDock Vina, with the receptor and ligand prepared as PDBQT files and the docking grid covering the active site of Drp1. The docking poses with the lowest binding energies were selected, and interactions such as hydrogen bonds and hydrophobic contacts were analyzed. PyMOL was used to visualize the binding conformations and key interaction sites.

Protein-protein docking and PISA analysis

The protein structures of Drp1 and Bax were retrieved from the UniProt database and prepared as PDB files. Structural optimization, including removal of water molecules and addition of hydrogen atoms, was performed using AutoDock Tools. Protein-protein docking was carried out using the PISA (Protein Interfaces, Surfaces and Assemblies) analysis tool to evaluate the interaction interface between Drp1 and Bax. PISA was employed to calculate binding free energy, interface area, and key residues involved in the interaction. The results were visualized in PyMOL to identify and analyze the binding interface, highlighting key interaction residues and structural conformations critical to the Drp1-Bax complex formation.

Mito-tracker red staining.

MitoTracker Red CMXRos (Beyotime, China), a cell-permeable X-rosaline derivative, was employed to label active mitochondria. Cells were incubated with the MitoTracker solution at 37 °C for 15 to 30 min. Following the replacement of the incubation medium with fresh culture medium, mitochondrial morphology and dimensions were visualized using an LSM700 Carl Zeiss confocal microscope (Jena, Germany).

Cellular ROS detection

DCFH-DA (Beyotime), a non-fluorescent probe, was utilized to measure cellular ROS. Once internalized by cells, DCFH-DA is converted by esterases to DCFH, which is then oxidized to fluorescent DCF in the presence

of ROS. Cells were incubated with DCFH-DA for 30 min, and fluorescence was subsequently monitored using an LSM700 Carl Zeiss confocal microscope (Jena, Germany).

MDA and SOD detection

Levels of MDA and SOD activity, serving as markers of oxidative stress, were quantified using assay kits (Beyotime) in accordance with the manufacturer's instructions.

Statistics

Data were expressed as mean \pm standard deviation (SD). Differences between experimental groups were analyzed using one-way ANOVA in GraphPad Prism 9.0 (GraphPad Software, La Jolla, CA, USA). Statistical significance was established at P-values less than 0.05 (*P<0.05; **P<0.01).

Data availability

The datasets generated and analyzed during the current study are available in the Sequence Read Archive(SRA) repository, PRJNA1146984.

Received: 10 August 2024; Accepted: 26 December 2024

Published online: 02 January 2025

References

- Li, Q. et al. Mitochondrial targeting of herbal medicine in chronic kidney disease. Front. Pharmacol. 12, 632388. https://doi.org/10.3389/fphar.2021.632388 (2021).
- 2. Yeh, T. H. et al. From acute to chronic: Unraveling the pathophysiological mechanisms of the progression from acute kidney injury to acute kidney disease to chronic kidney disease. *Int. J. Mol. Sci.* 25, 1755. https://doi.org/10.3390/ijms25031755 (2024).
- André, C. et al. The AKI-to-CKD transition: The role of uremic toxins. Int. J. Mol. Sci. 24, 16152. https://doi.org/10.3390/ijms2422
 16152 (2023).
- Tamargo, C. et al. Treatment of acute kidney injury: A review of current approaches and emerging innovations. J. Clin. Med. 13, 2455. https://doi.org/10.3390/jcm13092455 (2024).
- 5. Gameiro, J. et al. Acute kidney injury: From diagnosis to prevention and treatment strategies. J. Clin. Med. 9, 1704. https://doi.org/10.3390/jcm9061704 (2020).
- 6. Zhang, X. et al. Prebiotics enhance the biotransformation and bioavailability of ginsenosides in rats by modulating gut microbiota. *J. Ginseng Res.* 45, 334–343. https://doi.org/10/g8sh4b (2021).
- Chen, Q. et al. Ginsenoside Compound K ameliorates development of diabetic kidney disease through inhibiting TLR4 activation induced by microbially produced imidazole propionate. *Int. J. Mol. Sci.* 23, 12863. https://doi.org/10.3390/ijms232112863 (2022).
- Wu, C. Y. et al. IgA nephropathy benefits from compound K treatment by inhibiting NF-κB/NLRP3 inflammasome and enhancing autophagy and SIRT1. J. Immunol. 205, 202–212. https://doi.org/10.4049/jimmunol.1900284 (2020).
- 9. Hsu, W. H. et al. Compound K inhibits priming and mitochondria-associated activating signals of NLRP3 inflammasome in renal tubulointerstitial lesions. *Nephrol. Dial Transpl.* **35**, 74–85 (2020).
- 10. Zuo, Y. et al. Identification of matrix metalloproteinase-10 as a key mediator of podocyte injury and proteinuria. *Kidney Int.* **100**, 837–849. https://doi.org/10.1016/j.kint.2021.05.035(2021).
- 11. Li, J. et al. Research progress on exosomes in podocyte injury associated with diabetic kidney disease. Front. Endocrinol. 14 (1129884). https://doi.org/10.3389/fendo.2023.1129884 (2023).
- 12. Kriz, W. The inability of podocytes to proliferate: Cause, consequences, and origin. *Anat. Rec (Hoboken).* 303, 2588–2596. https://doi.org/10.1002/ar.24291 (2020).
- 13. Reynolds, P. A. The mechanobiology of kidney podocytes in health and disease. Clin. Sci. (Lond). 134, 1245–1253. https://doi.org/10.1042/CS20190764 (2020).
- Liu, S. et al. Podocyte injury in diabetic kidney disease: A focus on mitochondrial dysfunction. Front. Cell. Dev. Biol. 10 (832887). https://doi.org/10.3389/fcell.2022.832887 (2022).
- 15. Yu, C. J. et al. The pathophysiologic role of gelsolin in chronic kidney disease: Focus on podocytes. *Int. J. Mol. Sci.* 22, 13281 https://doi.org/10.3389/fcell.2022.832887 (2021).
- Huang, X. et al. PFKFB3 downregulation aggravates angiotensin II-induced podocyte detachment. Ren. Fail. 45, 2230318 https://doi.org/10.1080/0886022X.2023.2230318 (2023).
- 17. Yin, L. et al. Controversies in podocyte loss: Death or detachment? Front. Cell Dev. Biol. 9, 771931. https://doi.org/10.3389/fcell.2021.771931(2021).
- 18. Yamamoto, K. et al. Podocytes are lost from glomeruli before completing apoptosis. *Am. J. Physiol. Renal Physiol.* 323, F515–F526 https://doi.org/10.1152/ajprenal.00080.2022. (2022).
- Xing, L. et al. Astragaloside IV protects against podocyte apoptosis by inhibiting oxidative stress via activating PPARγ-Klotho-FOXO1 axis in diabetic nephropathy. Life Sci. 269, 119068. https://doi.org/10.1016/j.lfs.2021.119068(2021).
- Cao, Y. et al. MFN2 regulates high glucose-induced MAMs dysfunction and apoptosis in podocytes via PERK pathway. Front. Cell. Dev. Biol. 9 (769213). https://doi.org/10.3389/fcell.2021.769213.eCollection2021 (2021).
- 21. Erekat, N. S Programmed cell death in diabetic nephropathy: A review of apoptosis, autophagy, and necroptosis. *Med. Sci. Monit.* 28, e937766. https://doi.org/10.12659/MSM.937766(2022).
- 22. Zhu, Z. et al. Mitoquinone protects podocytes from angiotensin II-induced mitochondrial dysfunction and injury via the KEAP1-NRF2 signaling pathway. Oxid. Med. Cell Longev. 1394486 (2021). https://doi.org/10.1155/2021/1394486.eCollection2021 (2021).
- 23. Vida, C. et al. Oxidative stress in patients with advanced CKD and renal replacement therapy: The key role of peripheral blood leukocytes. *Antioxidants (Basel)* 10, 1155. https://doi.org/10.3390/antiox10071155 (2021).
- 24. Li, T. et al. Loss of MTX2 causes mitochondrial dysfunction, podocyte injury, nephrotic proteinuria and glomerulopathy in mice and patients. *Int. J. Biol. Sci.* 20, 937–952 (2024).
- 25. Vercellino, I. et al. The assembly, regulation and function of the mitochondrial respiratory chain. *Nat. Rev. Mol. Cell Biol.* 23, 141–161. https://doi.org/10/gnqvhv (2022).
- Mise, K. et al. NDUFS4 regulates cristae remodeling in diabetic kidney disease. Nat. Commun. 15, 1965. https://doi.org/10/gtkwnw (2024).
- 27. Geldon, S. et al. Redox-mediated regulation of mitochondrial biogenesis, dynamics, and respiratory chain assembly in yeast and human cells. Front. Cell. Dev. Biol. 9, 720656. https://doi.org/10.3389/fcell.2021.720656 (2021).
- Han, X. et al. Placental mesenchymal stem cells alleviate podocyte injury in diabetic kidney disease by modulating mitophagy via the SIRT1-PGC-1α-TFAM pathway. Int. J. Mol. Sci. 24, 4696. https://doi.org/10.3390/ijms24054696 (2023).

- Yapa, N. M. B. et al. Mitochondrial dynamics in health and disease. FEBS Lett. 595, 1184–1204. https://doi.org/10.1002/1873-346 8.14077 (2021).
- Adebayo, M. et al. Mitochondrial fusion and fission: The fine-tune balance for cellular homeostasis. FASEB J. 35 (e21620). https://doi.org/10.1096/fj.202100067R (2021).
- 31. Gao, S. et al. Complement C3a and C3a receptor activation mediates podocyte injuries in the mechanism of primary membranous nephropathy. *J. Am. Soc. Nephrol.* 33, 1742–1756. https://doi.org/10.1681/ASN.2021101384 (2022).
- 32. Gong, M. et al. Modified Hu-Lu-Ba-Wan protects diabetic glomerular podocytes via promoting PKM2-mediated mitochondrial dynamic homeostasis. *Phytomedicine* 123, 155247, https://doi.org/10.1016/j.phymed.2023.155247 (2024).
- 33. Jadli, A. et al. Abstract P176: Pharmacological inhibition of DRP1-dependent mitochondrial fission alleviates mitochondrial dysfunction-associated cell death in vascular smooth muscle cells. *Arterioscler. Thromb. Vasc Biol.* 41 (Suppl_1). https://doi.org/10.1161/atvb.41.suppl_1.P176 (2021).
- 34. Huang, S. et al. DDAH2 suppresses RLR-MAVS-mediated innate antiviral immunity by stimulating nitric oxide-activated, DRP1-induced mitochondrial fission. Sci. Signal. 14, eabc7931. https://doi.org/10.1126/scisignal.abc79 (2021).
- 35. Jenner, A. et al. DRP1 interacts directly with BAX to induce its activation and apoptosis. *EMBO J.* 41 (e108587). https://doi.org/10.15252/embj.2021108587 (2022).
- 36. Doblado, L. et al. Mitophagy in human diseases. Int. J. Mol. Sci. 22, 3903. https://doi.org/10.3390/ijms22083903 (2021).
- 37. Guo, H. et al. ADP-ribosylation factor-interacting protein 2 acts as a novel regulator of mitophagy and autophagy in podocytes in diabetic nephropathy. *Antioxid. (Basel).* **13**, 81 (2024).
- 38. Liu, B. et al. MitoTEMPO protects against podocyte injury by inhibiting NLRP3 inflammasome via PINK1/Parkin pathway-mediated mitophagy. Eur. J. Pharmacol. 929, 175136 (2022).
- 39. Wu, Y. et al. Poricoic acid a induces mitophagy to ameliorate podocyte injury in diabetic kidney disease via downregulating FUNDC1. I. Biochem. Mol. Toxicol. 37, e23503 (2023).
- 40. He, Y. et al. Deficient tRNA posttranscription modification dysregulated the mitochondrial quality controls and apoptosis. *iScience* 27, 108883 (2024).
- Khuanjing, T. et al. Donepezil attenuated cardiac ischemia/reperfusion injury through balancing mitochondrial dynamics, mitophagy, and autophagy. *Transl Res.* 230, 82–97. https://doi.org/10.1016/j.trsl.2020.10.010 (2021).
- Tian, T. et al. The role of DRP1-mediated mitophagy in HT22 cell apoptosis induced by silica nanoparticles. Ecotoxicol. Environ. Saf. 272, 116050 (2024).
- 43. Wu, F. et al. Bleomycin A5 suppresses DRP1-mediated mitochondrial fission and induces apoptosis in human nasal polyp-derived fibroblasts. *Int. J. Mol. Med.* 47, 346–360. https://doi.org/10.3892/ijmm.2020.4797 (2021).
- 44. Onishi, M. et al. Molecular mechanisms and physiological functions of mitophagy. EMBO J. 40 (e104705). https://doi.org/10.1525 2/embi.2020104705 (2021).
- Chen, M. et al. IRF-4 deficiency reduces inflammation and kidney fibrosis after folic acid-induced acute kidney injury. Int. Immunopharmacol. 100, 108142. https://doi.org/10.1016/j.intimp.2021.108142 (2021).
- 46. Zhou, Y. et al. MHC class II in renal tubules plays an essential role in renal fibrosis. *Cell. Mol. Immunol.* 18, 2530–2540. https://doi.org/10.1038/s41423-021-00763-z (2021).
- Yan, L. J. Folic acid-induced animal model of kidney disease. Anim. Models Exp. Med. 4, 329–342. https://doi.org/10.1002/ame2.1 2194 (2021).
- 48. Ning, L. et al. Synaptopodin is dispensable for normal podocyte homeostasis but is protective in the context of acute podocyte injury. *J. Am. Soc. Nephrol.* 31, 2815–2832. https://doi.org/10.1681/ASN.2020050572 (2020).
- 49. Barutta, F. et al. Mechanisms of podocyte injury and implications for diabetic nephropathy. Clin. Sci. (Lond). 136, 493–520. https://doi.org/10.1042/CS20210625 (2022).
- Tesch, F. et al. Super-resolved local recruitment of CLDN5 to filtration slits implicates a direct relationship with podocyte foot process effacement. J. Cell. Mol. Med. 25, 7631–7641. https://doi.org/10.1111/jcmm.16519 (2021).
- 51. Mundel, P. et al. Proteinuria: An enzymatic disease of the podocyte? Kidney Int. 77, 571–580. https://doi.org/10.1038/ki.2009.424 (2010).
- 52. Matsuda, J. et al. Rho GTPase regulatory proteins in podocytes. *Kidney Int.* 99, 336–345. https://doi.org/10.1016/j.kint.2020.08.035 (2021).
- 53. Foxman, E. et al. Rho GTPase regulatory proteins contribute to podocyte morphology and function. *McGill Sci. Undergrad. Res. J.* **2024**. https://doi.org/10.26443/msurj.v18i1.193 (2023).
- 54. Steichen, C. et al. Rho GTPases in kidney physiology and diseases. Small GTPases. 13, 141–161. https://doi.org/10.1080/21541248 .2021.1932402 (2022).
- 55. Li, Q. et al. Rho-GTPase activating protein myosin MYO9A identified as a novel candidate gene for monogenic focal segmental glomerulosclerosis. *Kidney Int.* **99**, 1102–1117. https://doi.org/10.1016/j.kint.2020.12.022 (2021).
- 56. Wu, N. S. et al. The mystery of phospho-DRP1 with four adaptors in cell cycle: When mitochondrial fission couples to cell fate decisions. *Cell. Cycle.* 22, 2485–2503. https://doi.org/10.1080/15384101.2023.2289753 (2023).
- 57. Fujiwara, N. et al. Autophagy regulates levels of tumor suppressor enzyme protein phosphatase 6. Cancer Sci. 111, 4371–4380
- 58. Kaur, S. et al. The beclin 1 interactome: Modification and roles in the pathology of autophagy-related disorders. *Biochimie* 175, 34–49. https://doi.org/10.1016/j.biochi.2020.04.025 (2020).
- Tian, F. et al. The ginsenoside metabolite compound K stimulates glucagon-like peptide-1 secretion in NCI-H716 cells by regulating the RhoA/ROCKs/YAP signaling pathway and cytoskeleton formation. J. Pharmacol. Sci. 145, 88–96. https://doi.org/1 0.1016/j.jphs.2020.11.005 (2021).
- Garg, P. et al. Actin-depolymerizing factor cofilin-1 is necessary in maintaining mature podocyte architecture. J. Biol. Chem. 285, 22676–22688. https://doi.org/10.1074/jbc.M110.122929 (2010).
- 61. Li, X. et al. Hhex inhibits cell migration via regulating RhoA/CDC42-CFL1 axis in human lung cancer cells. *Cell. Commun. Signal.* 19, 80. https://doi.org/10.1186/s12964-021-00763-6 (2021).
- 62. Bouslama, R. et al. Phosphorylation of PACSIN2 at S313 regulates podocyte architecture in coordination with N-WASP. *Cells* 12, 1487. https://doi.org/10.3390/cells12111487 (2023).
- Solanki, A. K. et al. Phosphorylation of slit diaphragm proteins nephrin and NEPH1 upon binding of HGF promotes podocyte repair. J. Biol. Chem. 297, 101079. https://doi.org/10.1016/j.jbc.2021.101079 (2021).
- 64. Ashworth, S. et al. Cofilin-1 inactivation leads to proteinuria—studies in zebrafish, mice and humans. PLoS One. 5, e12626 (2010).
- 65. Sousa-Squiavinato, A. C. M. et al. Cofilin-1, LIMK1 and SSH1 are differentially expressed in locally advanced colorectal cancer and according to consensus molecular subtypes. *Cancer Cell Int.* 21, 69. https://doi.org/10.1186/s12935-021-01770-w (2021).
- Li, H. et al. Dendrobium officinale polysaccharide decreases podocyte injury in diabetic nephropathy by regulating IRS-1/AKT signal and promoting mitophagy. Aging 15, 10291–10306. https://doi.org/10.18632/aging.205075 (2023).
- 67. Cao, J. et al. Endoplasmic reticulum stress and reactive oxygen species in plants. *Antioxid.* (Basel). 11, 1240. https://doi.org/10.339 0/antiox11071240 (2022).
- 68. He, J. et al. Redox regulation of autophagy in cancer: Mechanism, prevention and therapy. *Life (Basel)*. 13, 98. https://doi.org/10.3 390/life13010098 (2022).

- 69. Zhang, Y. et al. Caffeic acid phenethyl ester inhibits neuro-inflammation and oxidative stress following spinal cord injury by mitigating mitochondrial dysfunction via the SIRT1/PGC1α/DRP1 signaling pathway. *J. Transl Med.* 22, 304. https://doi.org/10.1 186/s12967-024-05089-8 (2024).
- Deragon, M. A. et al. Mitochondrial trafficking of MLKL, BAK/BAX, and DRP1 is mediated by RIP1 and ROS, which leads to decreased mitochondrial membrane integrity during the hyperglycemic shift to necroptosis. *Int. J. Mol. Sci.* 24, 8609. https://doi.org/10.3390/ijms24108609 (2023).
- Zang, N. et al. cGAS-STING activation contributes to podocyte injury in diabetic kidney disease. iScience 25, 105145. https://doi. org/10.1016/j.isci.2022.105145 (2022).
- 72. Hou, Y. et al. CD36 promotes NLRP3 inflammasome activation via the mtROS pathway in renal tubular epithelial cells of diabetic kidneys. *Cell. Death Dis.* 12, 523. https://doi.org/10/gk3xqk (2021).
- 73. Gao, Y. et al. ManNAc protects against podocyte pyroptosis via inhibiting mitochondrial damage and ROS/NLRP3 signaling pathway in diabetic kidney injury model. *Int. Immunopharmacol.* **107**, 108711 (2022).
- Li, G. et al. Syringaresinol protects against diabetic nephropathy by inhibiting pyroptosis via NRF2-mediated antioxidant pathway. Cell. Biol. Toxicol. 39, 621–639. https://doi.org/10.1007/s10565-023-09790-0 (2023).
- 75. Wu, S. et al. Bax is essential for DRP1-mediated mitochondrial fission but not for mitochondrial outer membrane permeabilization caused by photodynamic therapy. *J. Cell. Physiol.* 226, 530–541. https://doi.org/10.1002/jcp.22362 (2011).
- 76. Yang, C. C. et al. Repeated administration of adipose-derived mesenchymal stem cells added on beneficial effects of empagliflozin on protecting renal function in diabetic kidney disease rat. *Biomed. J.* 47, 100613. https://doi.org/10.1016/j.bj.2023.100613 (2023).
- 77. Yue, Y. et al. Intrarenal arterial administration of human umbilical cord-derived mesenchymal stem cells effectively preserved the residual renal function of diabetic kidney disease in rat. Stem Cell. Res. Ther. 13, 186. https://doi.org/10.1186/s13287-022-02857-5 (2022).
- 78. Lu, Y. P. et al. Empagliflozin reduces kidney fibrosis and improves kidney function by alternative macrophage activation in rats with 5/6-nephrectomy. *Biomed. Pharmacother.* **156**, 113947. https://doi.org/10.1016/j.biopha.2022.113947 (2022).

Acknowledgements

This project was supported by Discipline Construction Project of Zhejiang Chinese Medical University, the National Natural Science Foundation of China (No. 81803980), the Research Project of Zhejiang Chinese Medical University (No. 2022JKZZW03, 2020ZG09), and the Zhejiang Chinese Medicine University Postgraduate Scientific Research Fund Project (No. 2022YKJ03).

Author contributions

Huang FG designed the study, performed the experiments and wrote this manuscript. Huang S performed the experiments. Sun K performed the experiments and analyzed the data. Chen YH performed the experiments. Xie GQ and Bao J provided technical guidance and supervised the research. Fan YS secured the funding and reviewed the manuscript. All authors contributed to the article and approved the submitted version.

Declarations

Competing interests

The authors declare no competing interests.

Declaration of competing interest

The authors declare that they have no conflicts of interest.

Ethics statement

All experiments involving animals have been approved by the Institutional Animal Care and Use Committee of Zhejiang Chinese Medical University (the approval number of ethics committee: IACUC-20240429-16). All animal procedures were adhered to internationally accepted standards for animal research, following the 3Rs principle. The ARRIVE guidelines were employed for reporting experiments involving live animals, promoting ethical research practices.

Additional information

Supplementary Information The online version contains supplementary material available at https://doi.org/1 0.1038/s41598-024-84704-6.

Correspondence and requests for materials should be addressed to Y.F.

Reprints and permissions information is available at www.nature.com/reprints.

Publisher's note Springer Nature remains neutral with regard to jurisdictional claims in published maps and institutional affiliations.

Open Access This article is licensed under a Creative Commons Attribution-NonCommercial-NoDerivatives 4.0 International License, which permits any non-commercial use, sharing, distribution and reproduction in any medium or format, as long as you give appropriate credit to the original author(s) and the source, provide a link to the Creative Commons licence, and indicate if you modified the licensed material. You do not have permission under this licence to share adapted material derived from this article or parts of it. The images or other third party material in this article are included in the article's Creative Commons licence, unless indicated otherwise in a credit line to the material. If material is not included in the article's Creative Commons licence and your intended use is not permitted by statutory regulation or exceeds the permitted use, you will need to obtain permission directly from the copyright holder. To view a copy of this licence, visit http://creativecommons.org/licenses/by-nc-nd/4.0/.

© The Author(s) 2024